Structure, specific surface area and thermal conductivity of the snowpack around Barrow, Alaska

Florent Domine, Jean-Charles Gallet, Josué Bock, Samuel Morin

Structure, specific surface area and thermal conductivity of the snowpack around Barrow, Alaska

Florent Domine,[1,2] Jean-Charles Gallet,[1,3] Josué Bock,[1] and Samuel Morin[4]

Received 29 July 2011; revised 20 January 2012; accepted 23 January 2012; published 15 March 2012.

[1] The structure of the snowpack near Barrow was studied in March–April 2009. Vertical profiles of density, specific surface area (SSA) and thermal conductivity were measured on tundra, lakes and landfast ice. The average thickness was 41 cm on tundra and 21 cm on fast ice. Layers observed were diamond dust or recent wind drifts on top, overlaying wind slabs, occasional faceted crystals and melt-freeze crusts, and basal depth hoar layers. The top layer had a SSA between 45 and 224 $m^2\ kg^{-1}$. All layers at Barrow had SSAs higher than at many other places because of the geographical and climatic characteristics of Barrow. In particular, a given snow layer was remobilized several times by frequent winds, which resulted in SSA increases each time. The average snow area index (SAI, the dimensionless vertically integrated SSA) on tundra was 3260, higher than in the Canadian High Arctic or in the Alaskan taiga. This high SAI, combined with low snow temperatures, imply that the Barrow snowpack efficiently traps persistent organic pollutants, as illustrated with simple calculations for PCB 28 and PCB 180. The average thermal conductivity was 0.21 $Wm^{-1}\ K^{-1}$, and the average thermal resistance on tundra was 3.25 $m^2\ K\ W^{-1}$. This low value partly explains why the snow-ground interface was cold, around −19°C. The high SAI and low thermal resistance values illustrate the interplay between climate, snow physical properties, and their potential impact on atmospheric chemistry, and the need to describe these relationships in models of polar climate and atmospheric chemistry, especially in a climate change context.

Citation: Domine, F., J.-C. Gallet, J. Bock, and S. Morin (2012), Structure, specific surface area and thermal conductivity of the snowpack around Barrow, Alaska, *J. Geophys. Res.*, *117*, D00R14, doi:10.1029/2011JD016647.

1. Introduction

[2] It is now well established that the presence of snow on the ground impacts many environmental variables including (1) the energy budget of the surface because of the high snow albedo [*Hall*, 2004], (2) the energy budget of the ground because of the thermal insulation of the snowpack [*Zhang*, 2005], (3) the chemical reactivity of the atmospheric boundary layer, because snow is a photochemical reactor that releases numerous reactive species to the atmosphere, with the result that its oxidative capacity can be considerably increased [*Domine and Shepson*, 2002].

[3] All these impacts depend on snow physical properties and chemical composition. Albedo depends on the specific surface area (SSA, surface area per unit mass expressed in $m^2\ kg^{-1}$) and density of the snow layers that comprise the snowpack, as well as on the surface roughness of the snowpack and on its content in absorbing impurities [*Domine et al.*, 2008; *Warren et al.*, 1998]. The thermal effect of the snowpack depends of the thermal conductivity of the snow layers [*Sturm et al.*, 2002]. The chemical reactivity of the snowpack obviously depends on its chemical composition, but also on its physical properties, as detailed by *Domine et al.* [2008]. Briefly, the light flux is affected by snow SSA, as is the rate of reactions taking place on ice surfaces; the temperature profile in the snow, which affects chemical reaction rates, depends on the snow thermal conductivity, and the release of reaction products to the atmosphere depends on the snow surface structure and on its permeability.

[4] Given the potential impact of snow on atmospheric chemistry, the physical properties of the snowpack were studied at Barrow, on the Alaskan Arctic coast, during the OASIS09 field campaign. Variables studied were stratigraphy and snow type, specific surface area, density and thermal conductivity. Snow was studied on tundra, on lakes and on sea ice close to the coast (landfast ice). Temperature profiles in the snow on tundra were also monitored. To our knowledge, no detailed data on the SSA and thermal conductivity of the snowpack around Barrow have been published. *Dominé et al.* [2002] and *Cabanes et al.* [2003] report measurements of vertical profiles of snow SSA and of its rate of decrease at Alert, 82.5°N, in the Canadian high Arctic, but those data probably cannot be extrapolated to Barrow, because the warmer temperatures there result in a somewhat

[1]Laboratoire de Glaciologie et Géophysique de l'Environnement, CNRS-INSU and Université Joseph Fourier, Grenoble, France.
[2]Takuvik Joint International Laboratory, Université Laval and CNRS, Quebec, Quebec, Canada.
[3]Norwegian Polar Institute, Tromsø, Norway.
[4]Météo-France/CNRS, CNRM-GAME, CEN, St Martin d'Hères, France.

0148-0227/12/2011JD016647

different snowpack structure, including the presence of melt structures that are completely absent at Alert. There is no detailed data on thermal conductivity, even though model studies have calculated heat flux through snow on the Alaska North slope [*Ling and Zhang*, 2006, 2007]. *Derksen et al.* [2009] have reported detailed stratigraphic and density data over a 3000 km traverse in northern Alaska and Canada, but did not measure SSA or thermal conductivity.

2. Methods

2.1. Snow Observations and Density Measurements

[5] Standard snow pit techniques as described by *Dominé et al.* [2002] were used to observe snow stratigraphy. Briefly, a pit was dug and a clean vertical face was prepared. The use of a soft brush on this face helped reveal layer boundaries. Grain types, stratigraphy and hardness as defined by [*Fierz et al.*, 2009] were recorded. In some cases, photomacrographs of snow grains were taken with a digital reflex camera equipped with an inverted lens and extension tubes, as detailed by *Domine et al.* [2011b].

[6] Density was measured with density cutters [*Conger and McClung*, 2009]. For hard wind slabs or thin soft layers, a 100 cm^3 box-type steel cutter was used. For thick soft layers, a 500 cm^3 Plexiglass tube 6.5 cm in diameter beveled at one end was used. A snow fork was also tested [*Sihvola and Tiuri*, 1986]. This instrument uses radio waves to measure dielectric properties, from which snow density and liquid water content are derived. It is much faster and less tedious than density cutters. We found that data for wind slabs were similar to those obtained with density cutters. However, results were significantly lower for depth hoar, so that its use was not pursued. Furthermore, readings of 10% liquid water were sometimes obtained at temperatures as low as −30°C. This is presumably because of the strong ionic content of some snow layers affected by sea salt, but this was not tested in detail. All density data reported here are from density cutters, which have an accuracy around 10% [*Conger and McClung*, 2009].

2.2. Specific Surface Area Measurements

[7] SSA was measured using the DUFISSS (DUal Frequency Integrating Sphere for Snow SSA measurements) instrument [*Gallet et al.*, 2009]. A snow sample was obtained with a cylindrical corer and transferred with a piston to a sample holder 63 mm in diameter and 25 mm deep. A flat surface was cut and the sample holder was placed under the lower port of an integrating sphere 15 cm in diameter. Thin layers of diamond dust deposited on the surface were carefully sampled with a spatula into the sample holder, as detailed by *Domine et al.* [2011b]. Windborne snow was sampled by placing the sample holder in a shallow hole and letting the snow accumulate into it. The sample was illuminated with a 1310 or 1550 nm laser diode placed at the zenith. The 1550 nm wavelength was used for fresh, low density snow [*Gallet et al.*, 2009]. The reflected light was collected with the integrating sphere. The signal was measured with an InGaAs photodiode and converted to reflectance using a set of six standards of reflectances between 4 and 99%. The reflectance was converted to SSA using a calibration curve obtained with snow samples whose SSAs were measured using CH_4 adsorption and whose reflectances were measured with DUFISSS [*Gallet et al.*, 2009]. The accuracy of SSA measurements with DUFISSS is ±10%.

2.3. Thermal Conductivity Measurements

[8] The thermal conductivity of snow was measured with a TP02 heated needle probe from Hukseflux connected to a data logger, as detailed by *Morin et al.* [2010] and *Domine et al.* [2011a]. This measures the effective thermal conductivity, k_{eff}, which combines heat transfer by conduction through the network of interconnected ice crystals and through air in the pore space, and latent heat transfer caused by the temperature gradient in the snow. The heated needle probe method has been questioned by *Riche and Schneebeli* [2010], but those authors used it improperly and analyzed the part of the heated curve before a stationary regime was reached. Proper use of the method, i.e., if the first 30 to 60 s of the heating curve are discarded, yield meaningful data [*Morin et al.*, 2010]. Biases from this method are possible [*Calonne et al.*, 2011] and deserve further investigation, but the present data have undergone the quality checks described by *Morin et al.* [2010] and *Domine et al.* [2011a]. These are very similar to those of *Sturm et al.* [2002, 1997], so that comparisons are meaningful.

[9] To prevent heat exchanges due to ventilation, a tube 10 cm in diameter and 20 cm long was inserted in the snow. A metal blade was placed snugly at the far end of the tube to prevent airflow through the tube. If required by noticeable winds, a cap with a hole in its center was placed at the front end of the tube. The system was thermally stabilized for 5 to 10 min and a measurement sequence was started. In case of strong winds, measurements were made in a tent where large snow blocks of interest were transported and thermally equilibrated for 5 to 18 h before measurements. No detectable structural change is expected within that short time frame [*Flanner and Zender*, 2006; *Taillandier et al.*, 2007], since those blocks consisted of aged snow kept at temperatures below −20°C.

[10] The measurement sequence consisted of a 100 s baseline monitoring followed by 100 s of heating. The temperature difference ΔT between the center of the 10 cm-long heated region and the very end of the probe, 5 cm from the heated region, was monitored. The plot of ΔT versus ln(t), where t is time, showed a complex shape [*Sturm and Johnson*, 1992; *Morin et al.*, 2010], whose linear part has a slope proportional to $1/k_{eff}$. Based on the analysis detailed by *Morin et al.* [2010], and on calibration with glycerol and polyurethane foam, we estimate that our k_{eff} values are accurate within 10%.

3. Results

3.1. Tundra

[11] Snow on tundra was highly variable in thickness and stratigraphy, as already amply documented [e.g., *Derksen et al.*, 2009]. This is mostly because the uneven topography and vegetation catch blowing snow in a heterogeneous manner. To asses the short scale variability, a 12 m-wide trench was dug at 71°19.395′N, 156°39.685′W and its stratigraphy recorded. This is shown in Figure 1, where density values are also indicated. Snow symbols used are those of the International classification for seasonal snow on the ground [*Fierz et al.*, 2009]. In general, bottom layers are made of

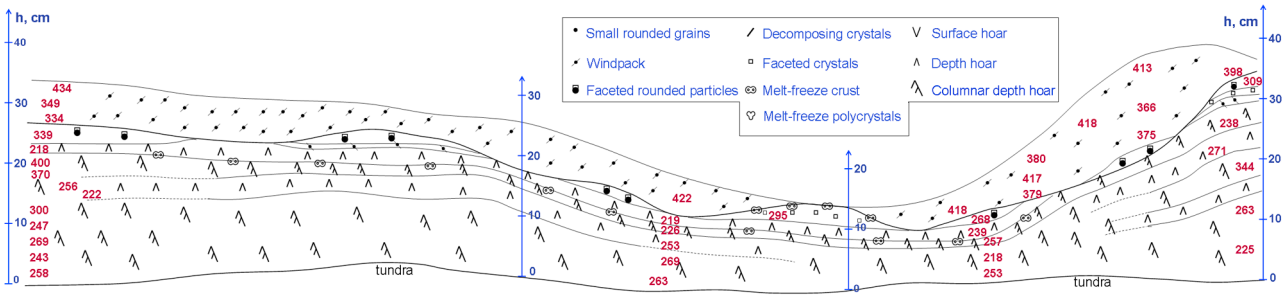

Figure 1. Snow stratigraphy on tundra near Barrow on 4 March 2009, along a 12 m-wide trench to show lateral variability. Horizontal and vertical scales are different. Red numbers are densities in kg m^{-3}, written where measurements were made. Snow crystal symbols are those used in this and subsequent figures.

depth hoar. Contrary to depth hoar in the taiga [*Taillandier et al.*, 2006] or in the high Arctic [*Dominé et al.*, 2002] the depth hoar here is often hard (indurated, i.e., it formed from a hard wind slab) and although large typical hollow and striated crystals are ubiquitous, small grains remain present, giving the depth hoar a milky aspect, much less transparent than in those other locations. Large crystals often are not individualized, producing clusters (Figure 2). In basal layers, depth hoar crystals are frequently aligned vertically, justifying the use of the symbol for "chains of depth hoar" (also called columnar depth hoar) in Figure 1. Again, this columnar depth hoar, which here is hard and in which a block can be carved and held up without falling apart, is often markedly different from that in the taiga [*Sturm and Benson*, 1997; *Taillandier et al.*, 2006], which falls apart at the first contact. Depth hoar densities range from 220 to 370 kg m^{-3} (one outlying value of 170 kg m^{-3} was found), while at Alert most values were in the range 190–230 kg m^{-3}. Intermediate layers are comprised of millimetric faceted crystal or faceting rounded grains. Upper layers are comprised of wind slabs, or of wind-drifts that have not yet sintered, sometimes topped by recent snow or diamond dust (i.e., clear sky precipitation [*Domine et al.*, 2011b; *Girard and Blanchet*, 2001; *Tape*, 1994]). Such drifts and fresh precipitation or condensation were not present on 4 March. Figure 1 shows that many layers are discontinuous and boundaries between layers shift laterally, appear and disappear, as already detailed by *Tape et al.* [2010]. This is because the stratigraphy is determined by wind and metamorphism more than by precipitation. The importance of wind is illustrated by the fact that between 28 February and 12 March, blowing snow was observed 8 out 13 days, while only one precipitation event took place. Thus, typically, a given snow fall is remobilized several times by wind before being covered. The effect of wind erosion is visible, as for example layers of faceted crystals are exposed in Figure 1. Last, one or two thin melt-freeze crusts were observed in most places. These layers were resistant to wind erosion, with the result that, after a wind event, they were exposed in many places, covering up to 20% of the surface. The nearby NOAA observatory's highest winter temperature was −1°C, and that was in December (http://www.esrl.noaa.gov/gmd/dv/data/?category=Meteorology&site=brw). Slight spatial temperature variations, freezing rain, or the freezing of supercooled droplets on the snow surface, generated by open leads in sea ice, may explain these crusts. Further illustrating the heterogeneity of the snowpack, Figure 3a shows the distribution of snowpack depths within a 400 m radius of this trench. 128 measurements were made, giving an average thickness of 41.4 cm.

[12] Specific surface area, density and thermal conductivity vertical profiles were measured in several spots picked at random on tundra, lakes and sea ice. Profiles and stratigraphy for two tundra sites are shown in Figure 4. More profiles are detailed in the auxiliary material.[1] The general trend is that SSA decreases with depth, with the average on land showing a monotonic decrease (Figure 5). Density and thermal conductivity profiles showed complex variations, with lower values near the bottom. The thermal conductivity of depth hoar reached 0.2 W m^{-1} K^{-1}, much higher than that of taiga depth hoar, which is in the range 0.03 to 0.1 [*Sturm and Johnson*, 1992].

[13] SSA, density and thermal conductivity showed large variations between sites. Figure 5 shows the ensemble of profiles of these three variables, along with the average profile, obtained by binning all values obtained within the depth

[1]Auxiliary materials are available in the HTML. doi:10.1029/2011JD016647.

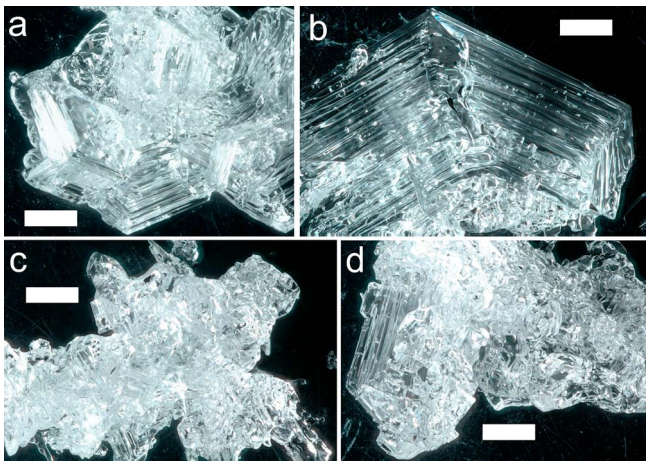

Figure 2. Depth hoar crystals in the basal layers of the Barrow snowpack. Scale bars: 1mm. (a) Clusters of hollow striated crystals are frequent. (b) Occasional large fairly pristine crystals, cup-shaped and striated coexist with (c and d) much smaller crystals with non-characteristic shapes.

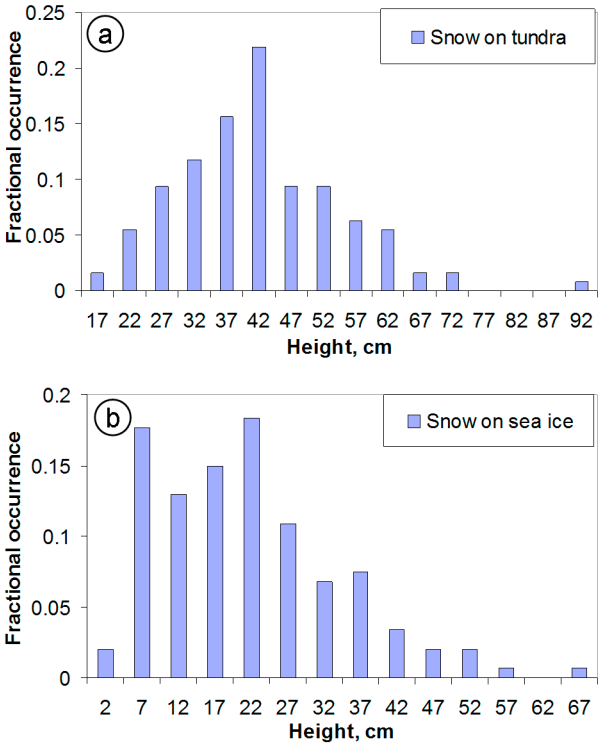

Figure 3. Distribution of the thickness of the snowpack. (a) On tundra (128 values) and (b) on sea ice (147 values). Each thickness interval spans 5 cm, e.g., the 27 cm class regroups thicknesses between 25.0 and 29.9 cm. The average values are 41.4 cm on tundra and 20.8 cm on sea ice.

ranges (in cm) [0–2.9], [3–6.9], [7–12.9], [13–20.9], [21–26.9], [27–34.9], [35–45.9] and [45–60]. For SSA and density, 8 vertical profiles are available on tundra. The statistical significance of these profiles was calculated with a Student's T test. The probability that a given SSA or density average is within 10% of the true average is between 65 and 91%, depending on depth (average 73%). If the margin of error is 20%, the probability rises to between 74 and 99% (average 86%). These average profiles reflect general observations well. The surface layer has a lower density and higher SSA than underlying layers because of the occasional presence of precipitation or recent wind drifts. Between 5 and 6 cm depths, there is a layer of SSA about 28 $m^2\ kg^{-1}$ and density 320 kg m^{-3} typical of the Barrow wind slab. Below 40 cm one finds a layer of SSA about 12 $m^2\ kg^{-1}$ and density 260 kg m^{-3} typical of the basal Barrow depth hoar. Between 16 and 40 cm depth there is a transition layer between the top wind slab and basal depth hoar, illustrating the variability of the wind slab thickness and the occasional presence of faceted crystals or of depth hoar layers not quite as evolved as the basal layer.

[14] For thermal conductivity, we only have four profiles on tundra (Figure 5c). The average on tundra, obtained by binning values into larger depth ranges, to obtain 6 values per range: [0–8.9], [9–13.9], [14–20.9], [21–27.9], [28–35.9] and [36–56] is shown. The statistical significance was again calculated as above. The probability to be within 20% of the true average value at a given depth is between 65 and 85% (average 72%). For an error less than 35%, the average probability is 86%. While this is clearly less favorable that for SSA and density, and considering the possible range of variation of snow thermal conductivity [*Sturm et al.*, 1997], we feel that these data are quite useful. The average profile shows values around 0.2 W $m^{-1}\ K^{-1}$ in the top 20 cm, typical of a fairly soft wind slab, and values around 0.13 between 30 and 40 cm, typical of the depth hoar at Barrow. The irregular shape of the profile near the top reflects the presence of a recent soft wind drift in the 27 March profile (Figure 4a) whose weight is exaggerated because of the small number

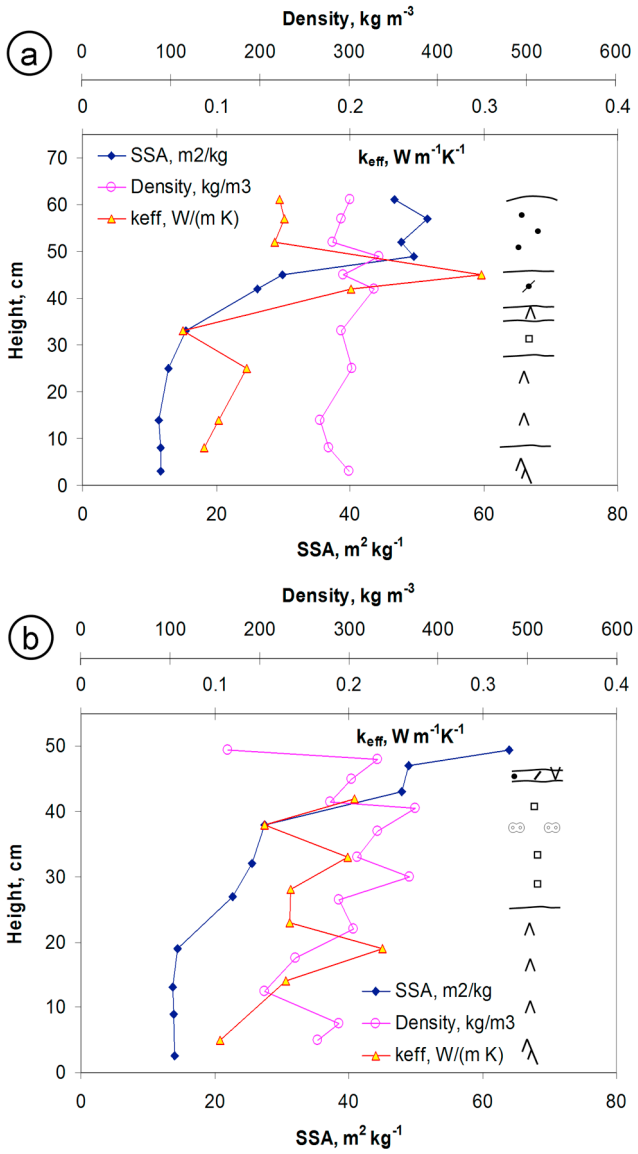

Figure 4. Profiles of specific surface area (SSA), density and thermal conductivity (k_{eff}) for snow on tundra. The stratigraphy is indicated on the side of the graphs, with the symbols of Figure 1. (a) On 27 March 2009 8 km South of Barrow, at 71°18.059′N, 156°46.042′W and (b) on 25 March 2009 near the trench of Figure 1. The top layer on Figure 4b is a mixture of decomposing particles, small rounded grains and surface hoar.

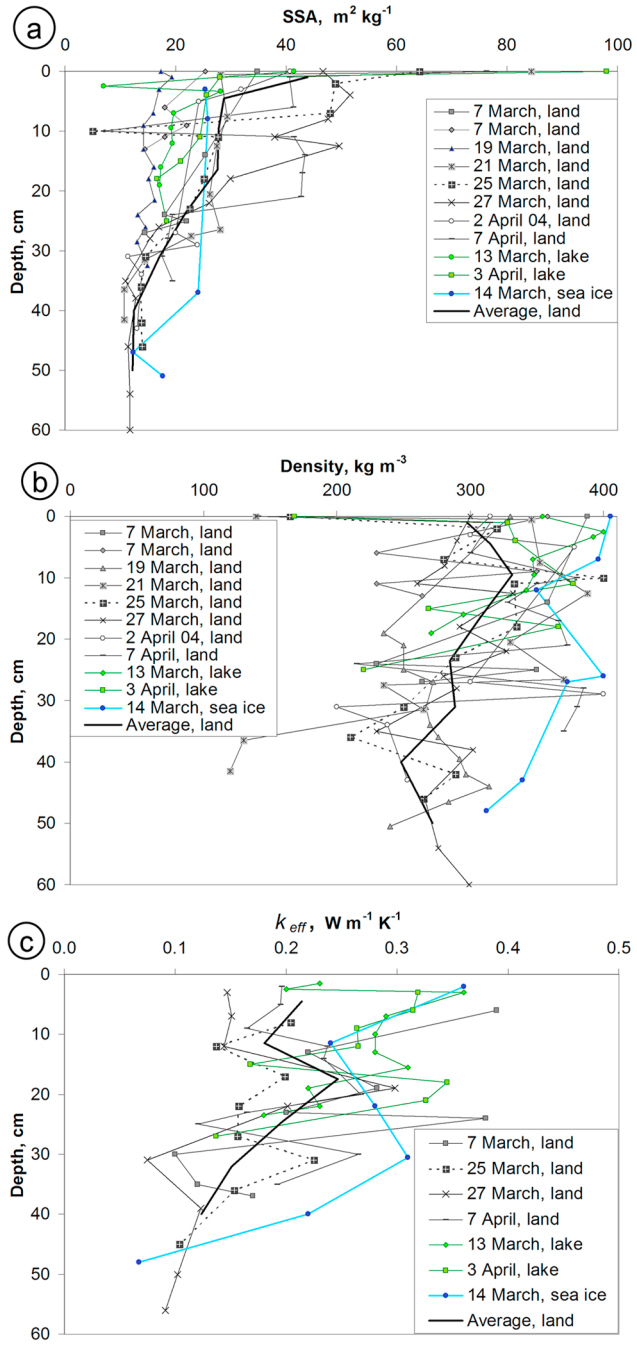

Figure 5. Variability of the vertical profiles of snow physical variables at Barrow in March – April 2009. (a) Specific surface area, (b) density and (c) thermal conductivity. Average profiles based on the pits studied on tundra are also shown.

of pits. We estimate that a more representative value in the top 20 cm would rather be around 0.25 W m^{-1} K^{-1}.

3.2. Lakes and Sea Ice

[15] Fewer data were obtained on lakes and sea ice than on tundra. The lake studied was just north of our regular study site, near the trench. There, the snow was spatially more homogeneous, likely because of the flat ice surface on which it deposited. On this lake, the snow depth was lower and less variable than on tundra, as already observed by *Sturm and Liston* [2003] and *Derksen et al.* [2009]. This is because (1) there is no vegetation or topography to catch blowing snow on lakes and (2) early snowfalls take place before freeze-up. Our own data are however insufficient to make a significant comparison of snow depth between lakes and tundra. The stratigraphy, density, SSA and thermal conductivity profiles on the lake are shown in Figure 6a. The snowpack featured essentially one 20 cm-thick layer changing continuously from columnar depth hoar at the base to faceted crystals at the top, all affected by a melting episode witnessed by the rounding of otherwise faceted crystal and the presence of typical melt-freeze clusters, sometimes

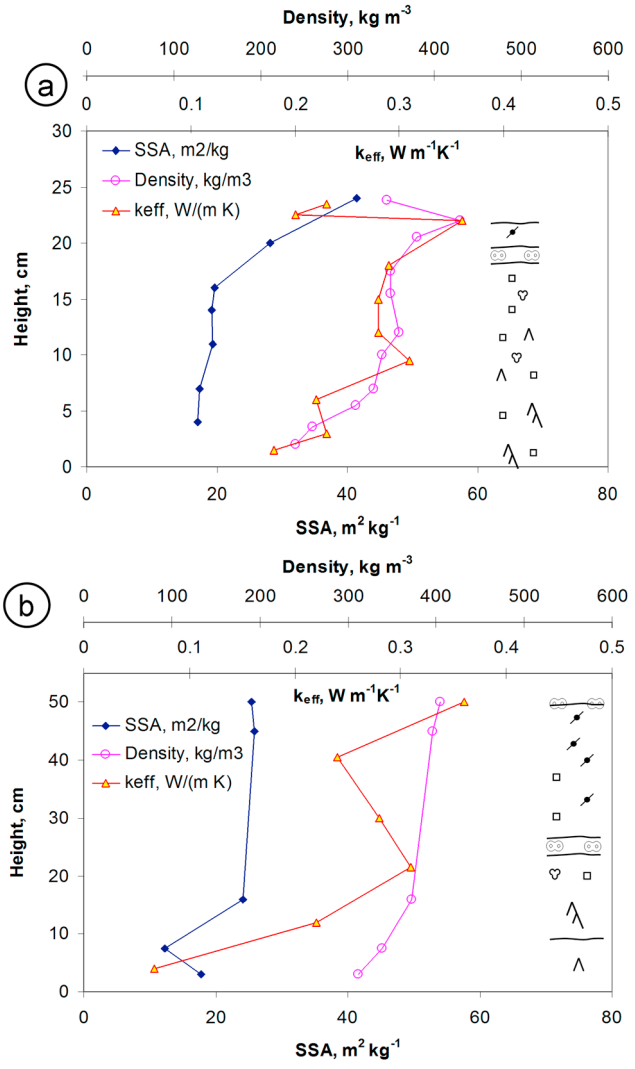

Figure 6. Profiles of specific surface area (SSA), density and thermal conductivity (k_{eff}) for snow on lake and sea ice. The stratigraphy is indicated on the side of the graphs. Note that the k_{eff} scale is different from that of Figure 4. (a) On 13 March 2009 on a lake just N of the trench of Figure 1 and (b) on 14 March 2009 on sea ice just N of point Barrow. In both cases, crystal shapes indicated that they had been subjected to slight melting, and this is indicated by the addition of the symbol for clustered melt-freeze crystals.

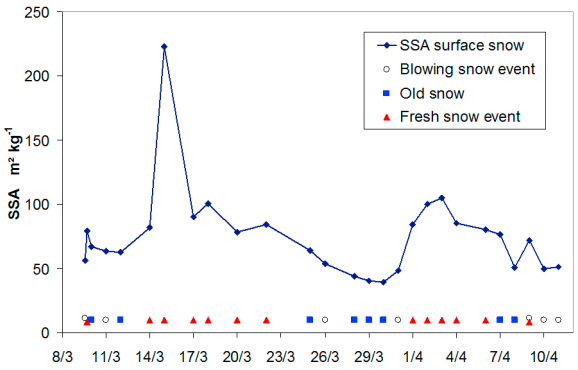

Figure 7. Specific surface area of the topmost snow layer (top 1 cm or less). Symbols above the *x* axis indicate the nature of this layer. Fresh snow was often a millimetric layer of diamond dust. The SSA of the blowing snow is that of captured airborne snow. Old snow is the most recent wind drifts, that usually covered 5 to 25% of the surface. The rest of the surface was then comprised of a variety of layers, including melt-freeze crusts of low SSA, not represented here.

faceted by subsequent metamorphism. A melt-freeze crust at the top of this layer separated it from a thin wind slab.

[16] Snow on sea ice was studied on landfast ice about 1 km off Point Barrow. There, the snow was highly heterogeneous, a common observation [*Dominé et al.*, 2002; *Sturm et al.*, 2002], with thicknesses (147 values) between 3 and 66 cm, and a mean value of 20.8 cm, exactly half the tundra value. The snow depth distribution (Figure 3b) is highly asymmetric. The stratigraphy was much more variable with the frequent complete absence of depth hoar or wind slabs. Melt-freeze crusts were much more frequent (1.8 per pit on average, versus 0.9 on land), possibly because of the more frequent presence of supercooled droplets coming from leads in the sea ice. Given the variability, it is not possible to produce a typical stratigraphy. That of Figure 6b, together with the SSA, density and thermal conductivity profiles that were measured, was obtained in a thick old snowdrift, whose age was attested by the partial transformation of the top wind slab into faceted crystals, as shown in Figure 6b. Because the DUFISSS system was not transported on site, the SSA of only a few samples that were brought back in boxes were measured. The flat SSA profile may be due to the small number of points, as we may have missed layers showing variations. The basal depth hoar layer was unusually soft and had a low thermal conductivity value (0.067 W m^{-1} K^{-1}).

3.3. SSA of the Very Surface Layer

[17] Figure 4b shows the presence of a thin surface layer of decomposing precipitation particles on which surface hoar has started to grow, with a SSA of 64 m^2 kg^{-1}. Clear sky precipitation (diamond dust) was frequent during the campaign, producing millimetric layers of high-SSA snow that grew up to 5 mm thick on windless periods. The density of this snow was 130 to 230 kg m^{-3} [*Domine et al.*, 2011b]. This surface layer is the most likely to interact with the atmosphere and its radiative impact is the highest, and we therefore report in Figure 7 the time variation of its SSA. All the precipitation was diamond dust except for the 9 March snow fall. On 1st April, a few scattered clouds and dendritic crystals were observed, so that precipitation was a mixture of diamond dust and snow. The diamond dust of 15 March was comprised of particularly small crystals [*Domine et al.*, 2011b], which explains its extremely high SSA. After wind events and in the absence of new precipitation (e.g., at the end of March), the snow surface was heterogeneous, with recent snow drifts alternating with older layers and even with melt-freeze crusts. Figure 7 reports the SSA of the recent snow drifts that formed the surface snow with the highest SSA. These drifts covered 5 to 25% of the surface, the rest of the surface being mostly wind slabs (SSA$\sim$30 m^2 kg^{-1}) and a melt freeze crust (SSA$\sim$10 m^2 kg^{-1}).

3.4. Snow Area Index

[18] The snow area index (SAI), defined by *Taillandier et al.* [2006], is the vertically integrated surface area available for gas adsorption in the snowpack. With the temperature profile in the snow, it serves to calculate the snowpack loading in chemical species that adsorb onto ice surfaces, such as poly chloro-biphenyls (PCBs) and other persistent organic pollutants (POPs). The SAI is calculated according to:

$$SAI = \sum_i SSA_i h_i \rho_i \quad (1)$$

where h_i is the thickness of layer i and ρ_i its density. SAI is a dimensionless variable that describes the factor by which snow multiplies the ground geometric surface area. Table 1 shows the 7 SAI values measured on tundra in March–April 2009, as well as one value in April 2004, when SSA was measured using CH_4 adsorption. On tundra, SAI_{tundra} = 3259 with a standard deviation of 1166. These values are probably fairly well representative of the SAI on tundra, as the average snow thickness is close to that obtained from Figure 3. There are insufficient values on lakes and sea ice to be representative. Since for a given snow type SSA values were similar on tundra, lakes and sea ice, SAI differences will be mostly governed by snow thickness. We then expect the SAI to be lower on lakes than on tundra. On sea ice, the variability in snowpack thickness and structure means that a much larger number of profiles must be measured for a

Table 1. Snow Area Index (SAI) for the Snowpacks Studied During This Campaign and in 2004

Location	Date	Snow Thickness (cm)	SAI
Tundra	7 March	47	3641
Tundra	7 March	32	1629
Tundra	19 March	35	1446
Tundra	21 March	47	3285
Tundra	25 March	50	3707
Tundra	27 March	64	4709
Tundra	7 April	39	4318
Tundra	2 April 2004	45	3333
	Average $\pm$ σ[a]	45 $\pm$ 10	3259 $\pm$ 1166
Lake	13 March	25	1833
Lake	3 April	31	2257
Sea ice	14 March	13	808
Sea ice	14 March	53	4260

[a]Only the average and standard deviation for data obtained on tundra are shown, as data on lakes and sea ice are not sufficient for statistics.

Table 2. Thermal Resistance R_T for the Snowpacks Studied During This Campaign

Location	Date	Snow Thickness (cm)	R_T (m^2 K W^{-1})
Tundra	7 March	45[a]	2.36
Tundra	25 March	50	3.36
Tundra	27 March	61[a]	5.12
Tundra	7 April	39	2.14
	Average $\pm$ σ[b]	49 $\pm$ 9	3.25 $\pm$ 1.36
Lake	13 March	25	1.02
Lake	3 April	31	1.40
Sea ice	14 March	13	0.84
Sea ice	14 March	50[a]	3.05

[a]These values are slightly different from those of Table 1 because measurements were made about 50 cm away, where snowpack thickness was different.
[b]Only the average and standard deviation for data obtained on tundra are shown, as data on lakes and sea ice are not sufficient for statistics.

representative value. If we base SAI estimates on snow thickness, Figure 3 indicates that SAI on sea ice should be about half the tundra value. The high value of 4260 calculated on sea ice is just because this spot has an unusual large accumulation of snow.

3.5. Thermal Resistance

[19] Just like the SAI can be used to characterize the specific surface area properties of the whole snowpack, the thermal resistance R_T can be used to characterize its thermal properties. This variable is defined as:

$$R_T = \sum_i \frac{h_i}{k_{eff,i}} \quad (2)$$

where h_i is the thickness of layer i and k_{eff} its thermal conductivity. R_T thus has units of m^2 K W^{-1} and this variable can be used conveniently to relate the upward heat flux through the snowpack F to the temperature difference between its surface and its base, T_{top}-T_{base}:

$$F = -\frac{T_{top} - T_{base}}{R_T} \quad (3)$$

Table 2 sums up the 8 R_T values measured. Based on 4 values, the average R_T value for tundra near Barrow is 3.25 m^2 K W^{-1}. Although four profiles have a limited statistical value as quantified above, Table 2 suggests that R_T is lower on lakes than on tundra, in line with the estimations of *Sturm and Liston* [2003], who calculated R_T from density-k_{eff} empirical relationships. Based on the lower snow thickness and on Table 2, we speculate that R_T is also lower on sea ice than on tundra.

4. Discussion

4.1. Conditions of Formation and Snow Properties

4.1.1. Meteorological Conditions at Barrow

[20] The snowpack near Barrow is typically Arctic [*Sturm et al.*, 1995] and shares many characteristics with that of Alert [*Dominé et al.*, 2002]. However, Alert has a much colder climate and several noteworthy differences deserve discussion to illustrate the impact of climate on the properties of the Arctic snowpack. Figure 8a shows the wind speed at

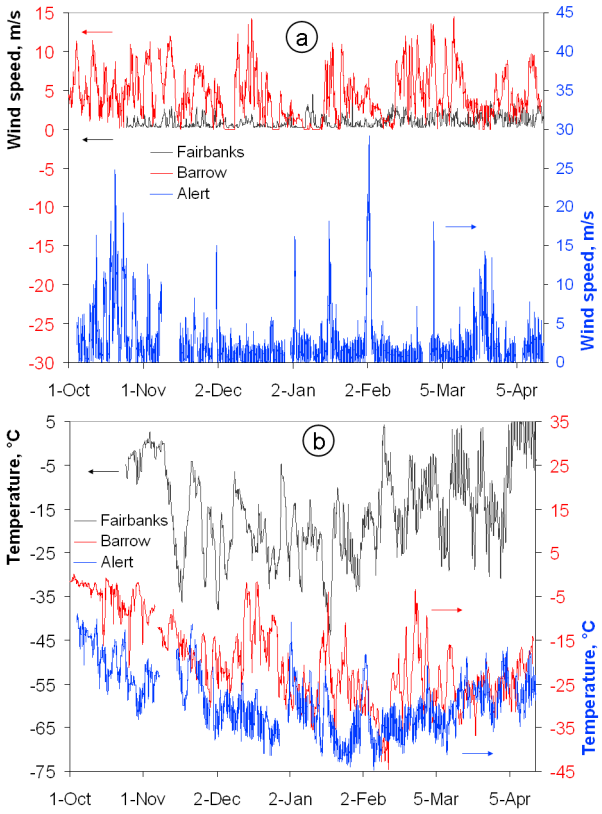

Figure 8. Comparison of wind speed at 2 m and temperature for Barrow (2008–2009), Fairbanks (2003–2004) and Alert (1999–2000). (a) Wind speed and (b) temperature.

2 m during the whole winter season for 3 sites: Barrow in 2008–2009, Alert in 1999–2000 [*Dominé et al.*, 2002] and Fairbanks in 2003–2004 [*Taillandier et al.*, 2006]. The Barrow wind speed available at the Barrow NOAA observatory was at 10 m height (http://www.esrl.noaa.gov/gmd/dv/data/?category=Meteorology&site=brw). For comparison with other sites, it was corrected to 2 m assuming a logarithmic wind speed profile and a drag coefficient of 0.0015. The temperature at the same 3 sites is shown in Figure 8b.

[21] It is interesting to compare meteorological data between Alert in 1999 and Barrow in 2008 between October, 1st about the date of the first snow, and December, 31st when the snowpack characteristics are established. This is done in Table 3. It is 13°C colder at Alert and 1.8 m s^{-1} windier at

Table 3. Comparison of Temperature and Wind Speed at 2 m During the OASIS 2009 and Alert 2000 Campaigns

	Barrow 2008–2009	Alert 1999–2000
Mean Temperature 1st Oct. to 31st Dec.	−12.3°C	−25.4°C
Mean Temperature 1st Jan. to 1st Mar.	−26.0°C	−33.2°C
Mean wind speed 1st Oct. to 31st Dec.	4.72 $\pm$ 3.02 m/s[a]	2.99 $\pm$ 3.66 m/s[a]
Mean wind speed 1st Jan. to 1st Mar.	3.75 $\pm$ 3.11 m/s[a]	2.42 $\pm$ 3.64 m/s[a]

[a]The standard deviation of wind speed is also shown.

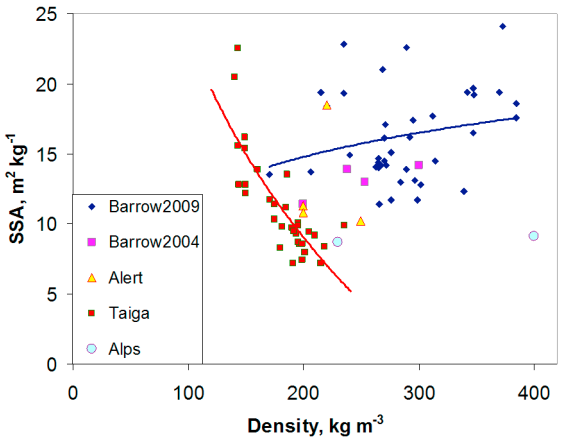

Figure 9. SSA-density correlations for depth hoar from the taiga [*Taillandier et al.*, 2006] and from this campaign. A few data points from Alert, a previous Barrow campaign and the Alps are also shown. Logarithmic fits to Taiga data and to the Barrow 2009 data are shown (equations (4) and (5)).

Barrow. However, the wind speed pattern is different at Alert, with periods of very high wind speeds alternating with calm periods, while moderate wind is frequent at Barrow. This is visible in the wind speed standard deviation, which is higher at Alert (Table 3). In autumn, wind speed exceeded 15 m s^{-1} on 4 occasions at Alert, including once for almost 24 h, while such speeds were never reached at Barrow. These different meteorological conditions must result in different snow properties that should be detectable in each of the snow layers studied at Barrow.

4.1.2. Specificity of the Depth Hoar at Barrow

[22] The colder autumn temperatures most likely induced a higher temperature gradient in the snowpack at Alert. In the Arctic, depth hoar can form in early season directly from precipitating layers undisturbed or little disturbed by wind. In that case, wind compaction does not take place and depth hoar density is low, usually below 200 kg m^{-3}. Most of the time, however, Arctic depth hoar forms from hard wind slabs that lose mass by sublimation of the warmer snow into the colder air above [*Derksen et al.*, 2009; *Dominé et al.*, 2002; *Sturm et al.*, 1995]. The resulting water vapor fluxes induce the growth of large depth hoar crystals. The comparison of our observations at Alert, where depth hoar of densities around 200 kg m^{-3} was prevalent, and Barrow indicate that the temperature gradients are not sufficient at Barrow to produce the mass loss by sublimation required to lower the density to 200 kg m^{-3} seen at Alert. Crystals therefore cannot grow as much in the denser matrix, because of lack of space and of slower growth kinetics. *Flanner and Zender* [2006] indeed calculate that in the temperature gradient metamorphic regime, the crystal growth rate decreases as density increases, and even ceases for densities greater than 480 kg m^{-3}. Apparently, the water vapor flux is spatially heterogeneous at the cm scale and does not affect some areas, where growth does not take place as rapidly (Figure 2c). The depth hoar at Barrow is therefore denser, has a higher SSA, is harder, and has stronger mechanical properties than at Alert. We also expect properties different from taiga depth hoar, since conditions of formation are different there [*Sturm and Benson*, 1997; *Taillandier et al.*, 2006]. Snow is not compacted by wind in the taiga (Figure 8a shows that wind speed near Fairbanks, a typical taiga site, seldom exceeded 3 m/s in 2003–2004), and depth hoar development takes place in snow whose density is around 200 kg m^{-3}, without initial stages with wind compaction and significant mass loss.

[23] It is therefore of interest to compare the relationships between physical properties of different depth hoars formed under different climatic conditions. Figure 9 shows the correlation between SSA and density for depth hoar from the taiga (near Fairbanks, interior Alaska) [*Domine et al.*, 2007a] and from this campaign. A few points obtained at Alert, during a previous campaign at Barrow, and in the Alps are also shown. Those previous SSA data were obtained using the lengthy CH_4 adsorption technique [*Legagneux et al.*, 2002], so they are few.

[24] The trends of the taiga and of Barrow are clearly different. Fits to a logarithmic equation, as done by *Domine et al.* [2007a] yield:

$$\mathrm{SSA_{taiga}} = -20.648\ \mathrm{Ln}(\rho_{snow}) + 118.44 \qquad (4)$$

where ρ_{snow} is the snow density, with a good correlation ($R^2 = 0.658$). For this campaign, we obtain:

$$\mathrm{SSA_{Barrow}} = 4.236\ \mathrm{Ln}(\rho_{snow}) - 7.6604 \qquad (5)$$

with hardly any correlation ($R^2 = 0.053$). Units are those of Figure 9. Note that the constant in equation (4) is different from that shown by *Domine et al.* [2007a] because they used different units.

[25] In the taiga, a correlation is expected because compaction due to destructive metamorphism and the weight of subsequent snow layers increase the density, concomitantly with depth hoar formation, which, like any snow grain growth, leads to a SSA decrease [*Taillandier et al.*, 2007]. In the tundra, on the contrary, initial wind compaction means that depth hoar develops after, not during, compaction, and this essentially takes place at constant or decreasing density. This last feature may in fact explain the slightly positive slope in equation (5), as over time, a decrease in both density and SSA are expected.

[26] The variability in the depth hoar densities at Barrow is probably due to the different densities of the wind slabs from which they formed, and these were determined by the different wind speeds that formed those wind slabs. The variability in SSA is due to several factors, including the value of the temperature gradient, the age of the snow, and its density [*Flanner and Zender*, 2006], so that there is no clear and unique link between SSA and density. As already stressed by *Domine et al.* [2007a], there is no good correlation between snow density and SSA in general. For a good correlation to appear, the snow type (e.g., depth hoar or wind slab) must be considered. Furthermore, Figure 9 (and also Figure 10 discussed below) indicates that, in addition to snow type, climatic conditions, play in crucial role in determining the SSA-density relationship and ideally the climatic zone should also be considered. Stressing the difference between depth hoars from the taiga in interior Alaska and from Barrow, the mean (density, SSA) values are (288, 16.2) for Barrow and (182, 11.2) for the taiga. Given the poor correlation for equation (5), it probably makes more sense, if a SSA value

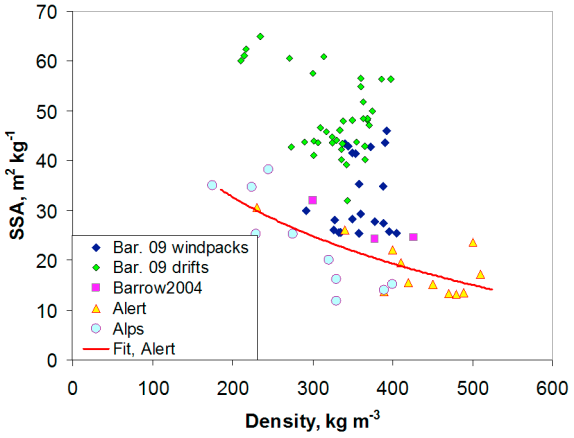

Figure 10. SSA-density correlations for wind slabs from several locations and from wind drifts at Barrow. The data from Alert and the Alps are from *Domine et al.* [2007a]. The equation of the Alert fit is SSA = $-19.264 \ln(\rho_{snow}) + 134.74$.

for depth hoar at Barrow is to be used in models, to simply use the average, 16.2 m^2 kg^{-1}, rather than equation (5). The few data points from Alert and Barrow 2004 do not show any significantly different trend from this campaign. The two points from the Alps are just informative, they are too few to even make statistics.

4.1.3. Specificity of the Wind Slabs and Wind Drifts at Barrow

[27] At Barrow, depth hoar forms mostly in autumn when temperature gradients in the snowpack are high, while wind slabs form in winter, once these gradients are reduced because the ground has cooled and the snowpack is thicker [*Dominé et al.*, 2002]. Wind slabs form from drifted snow, which is initially soft. The evolution of wind drifts at Barrow appeared to depend on their density, which is itself an increasing function of wind speed. The denser wind drifts would sinter to hard wind slabs in a few days, while the lighter ones would remain soft, sometimes even showing faceting crystals after a few days. Blowing snow appeared above a threshold of 5 to 7 m s^{-1}, depending on the cohesion of the surface snow. Given the wind time series of Figure 8a, new wind drifts were very frequent at Barrow. This is illustrated in Figure 11. Between 5 and 13 March, there was almost constant blowing snow and no precipitation. Drifts formed and were eroded constantly, indicating that a given snow layer was remobilized several times before forming a stable wind drift. Many of these had a density <300 kg m^{-3} because of the moderate wind speeds. In comparison, recent wind drifts were much rarer at Alert and had densities almost always >400 kg m^{-3}, a value seldom reached at Barrow.

[28] These differences of course manifest themselves in the SSA-density relationships, shown in Figure 10. For Barrow, we have differentiated the recent wind drifts (<4 days old) from the older, sintered wind slabs. It is clear that the Barrow wind slabs have a higher SSA that those at Alert. The fit to the Alert data is that already shown by *Domine et al.* [2007a]. The wind drifts have a very high SSA, due to the fact that when several consecutive days of drifting snow were taking place, as was the case between 5 and 13 March (Figure 11), snow would be deposited and remobilized several times in a row, and each time, this resulted in a SSA increase due to grain fragmentation and sublimation [*Domine et al.*, 2009]. In fact, the SSA of wind drifts at Barrow reach 65 m^2 kg^{-1}, an exceptionally high value for non-precipitating snow [*Domine et al.*, 2007a].

[29] Given the scatter in the SSA values of wind drifts and wind slabs at Barrow, it does not seem sensible to propose SSA-density correlations. The age of the drift or wind slab is also an important variable. The highest values are for recent drifts, while the lowest are for aged wind slabs. Aged wind slabs (>10 days old) have SSAs around 28 m^2 kg^{-1}. Wind slabs between 5 and 10 days old have SSAs around 43 m^2 kg^{-1}, while wind drifts 4 days old or less have SSAs between 45 and 65 m^2 kg^{-1}. A more thorough analysis of density-age-SSA relationships is required to propose equations predicting the SSA of these snows.

[30] The SSAs of Alpine wind slabs and layers of small rounded grains from the Alps [*Domine et al.*, 2007a] are also shown for comparison. The conclusion of Figure 10 is that Barrow wind slabs and wind drifts have a higher SSA than those from other places where they have been studied. Our interpretation is that the frequent winds remobilize snow many times and that each time an SSA increase takes place. After deposition, SSA decreases due to metamorphic effects that include sintering, but often, another erosion stage stops this decrease. On the contrary, the much rarer wind events at Alert, and the much greater accumulation in the Alps, which buries and protects layers from wind, results in snow being subjected to much fewer drifting events, so that SSA essentially decreases over time.

4.1.4. Specificity of the Very Surface Layer at Barrow

[31] After a wind event, the very surface layer at Barrow was heterogeneous. It typically consisted of many exposed layers that included several recent wind drifts, older layers that were often aged wind slabs but could also be layers of faceted crystals or depth hoar, and melt-freeze crusts. Based on Figure 7 and on estimates of the fraction of the surface covered by each snow type, we evaluate that the average SSA for the very surface layer after a wind event is most likely greater than 30 m^2 kg^{-1}.

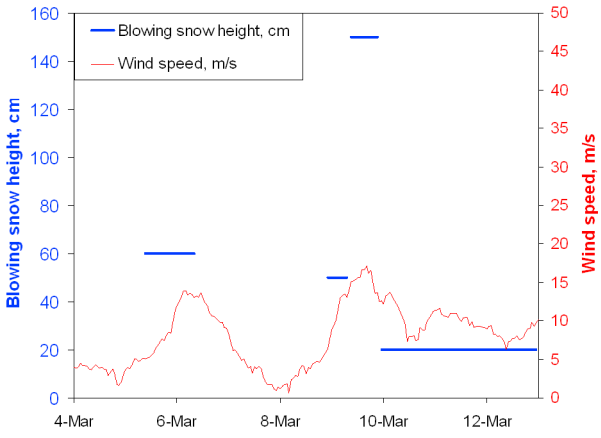

Figure 11. Wind speed and blowing snow height at Barrow between 4 and 13 March 2009. Blowing snow height is a visual estimate made twice a day, so that this variable is shown with a 12 h time resolution.

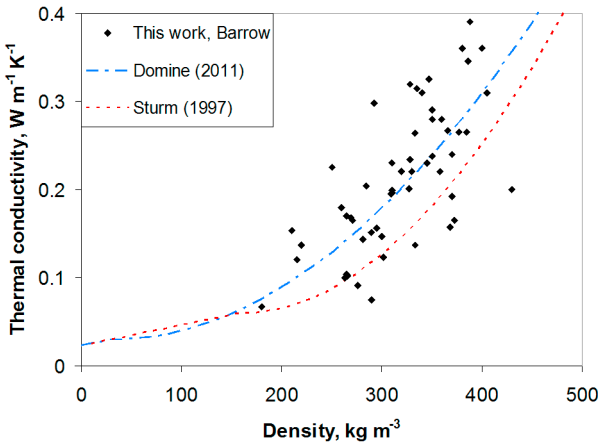

Figure 12. Correlation between thermal conductivity and density. Our data are compared with the quadratic equations of *Sturm et al.* [1997] and *Domine et al.* [2011a].

[32] During calm periods such as 13 to 25 March, diamond dust precipitation was often taking place, resulting in a surface layer of SSA > 80 m^2 kg^{-1} (Figure 7). As suggested by *Domine et al.* [2011b], we believe that the frequency of these diamond dust events is increased by the frequent presence of open water off Barrow, which produced massive input of water vapor to the atmosphere, as evidenced by thick clouds above the leads in sea ice. Although there are no published time series of surface snow SSA in other places, our experience suggests the SSA of the very surface layer is higher at Barrow than at Alert, in the taiga near Fairbanks and in the Alps. This is because (1) precipitation is much less frequent at Alert, in part because there is seldom open water nearby, (2) there is less frequent precipitation near Fairbanks, (3) even if some Alpine sites experience frequent precipitation, the warmer temperatures result in a fast SSA decrease [*Taillandier et al.*, 2007].

[33] In conclusion to the SSA of the various layers in the Barrow snowpack, the data presented indicate that each layer at Barrow has a higher SSA than equivalent layers at other sites where similar measurements have been made such as Alert, the Alaska taiga, and the Alps. This is because of the peculiar geography and climatic conditions at Barrow. Frequent open leads in sea ice due to interactions between winds and the shape of the coast line produce frequent, although non abundant, precipitation, resulting in a high SSA of the surface layer. Frequent winds, although moderate, remobilize a given snow fall many times and maintain a high SSA of drifts and wind slabs in the winter. Frequent winds and temperatures warmer than in the higher Arctic produce depth hoar of high density and reduce the temperature gradient in the snow, limiting the decrease in SSA of the depth hoar in autumn. These physical characteristics imply that the Barrow snowpack has a greater potential to adsorb reactants and catalyze chemical reactions than other snowpacks. Furthermore, since SSA and albedo are linked [*Domine et al.*, 2006], the Barrow snowpack may have a higher albedo than elsewhere. A final conclusion on this is not possible because albedo also depends on the impurity content [*Warren and Wiscombe*, 1980], which we do not study here. This higher albedo would result in higher actinic fluxes above the snow, again enhancing chemical reactions in the atmosphere.

4.1.5. Thermal Conductivity of the Snow at Barrow

[34] We have fewer thermal conductivity data than for SSA, so detailed discussions by snow types are not possible. A frequently shown correlation is that between thermal conductivity and density, which we report in Figure 12. Our data appear consistent with the quadratic equations of *Sturm et al.* [1997] and *Domine et al.* [2011a]. It is noteworthy to mention that the present data are for the most part (46 out of 55 points) different from those of *Domine et al.* [2011a], whose main purpose was to correlate thermal conductivity, shear resistance and density. As detailed by *Domine et al.* [2011a], the differences between the three data sets can simply be explained by different samplings in similar populations. In any case, the scatter in our data confirms once more that density alone is not a good predictor of thermal conductivity. The average k_{eff} value from our measurements is 0.21 W m^{-1} K^{-1}. Thus, the peculiarity of the snow at Barrow evidenced from its SSA does not appear to manifest itself in its density–thermal conductivity relationship.

4.2. Pollutant Adsorption By the Snowpack

[35] Table 1 show that the SAI on land at Barrow was 3259 ± 1166. In comparison, the SAI measured at Alert on tundra, based on 2 values, was 2230 [*Dominé et al.*, 2002]. In the taiga near Fairbanks, Alaska, the season-long monitoring of *Taillandier et al.* [2006] showed a peak value in late November of 1460, and SAI was near 1000 throughout winter until the onset of snowmelt. The high value obtained on tundra near Barrow was expected from the preceding section. It is due to the fact that (1) snow thickness is slightly greater than at Alert; (2) a large fraction of the snowpack consists of wind slabs, that have a higher density and higher SSA than depth hoar; (3) the depth hoar at Barrow has a higher SSA than that in the taiga because of its different formation process, as discussed above; (4) wind slabs at Barrow have a higher SSA than at Alert or in the Alps.

[36] Using temperature profiles that we measured, we compared its ability to retain pollutants such as PCBs, as done by *Taillandier et al.* [2006]. We retain the hypotheses made by those authors. They took the example of the fairly

Table 4. Calculated Distribution of PCB 28 and PCB 180 Between a 400 m-Thick Boundary Layer and the Snowpack for Three Locations

Location	Air T (°C)	Snow Surface T (°C)	Snow Bottom T (°C)	Snowpack SAI	PCB 28 Fraction in Snow (%)	PCB 180 Fraction in Snow (%)
Barrow, 21 March 2009	−26	−27	−20	3285	96.1	99.9
Fairbanks, 25 March 2004	−16	−17.3	−5.5	938	28.7	93.9
Alert, 18 April 2000	−26	−27	−27	2525	93.8	99.8

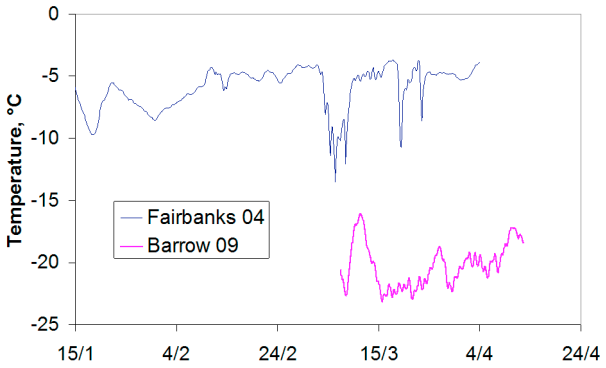

Figure 13. Comparison between the snow temperature in Fairbanks at a height of 7.5 cm above ground in 2004 with the snow temperature at Barrow at a height of 8 cm in 2009.

volatile PCB 28 (with 3 chlorine atoms) and of the low volatility PCB 180 (with 7 chlorine atoms). They assumed that PCBs adsorb to snow crystal surfaces according to an adsorption coefficient that follows a Henry's law, whose temperature variations are calculated with the adsorption enthalpy (−79.9 and −95.7 kJ mol^{-1} for PCB 28 and PCB 180, respectively. Table 4 sums up the results, which are also compared to similar calculations made for Alert (82°30′N [*Dominé et al.*, 2002]) and Fairbanks (65°N [*Taillandier et al.*, 2006]). Clearly, the Barrow snowpack, because of its high SAI and its cold temperature, traps most of the PCB of the (boundary layer + snow) system, even for the fairly volatile PCB 28. These calculations illustrate the potential of snowpacks to act as a reservoir of contaminants.

4.3. Thermal Insulation of the Tundra

[37] The average value of R_T on tundra (Table 2), 3.25 m^2 K W^{-1}, is lower than found in other snowpacks. For example, in the taiga, the work of *Sturm and Johnson* [1992] allows us to estimate R_T values around 6.2 m^2 K W^{-1}, using an average k_{eff} value of 0.065 W m^{-1} K^{-1} and a snowpack thickness of 40 cm. From measurements carried out in the Alps at an altitude of ca. 2400 m on 18 February 2009, in a snowpack typical of the Alpine type and 1.6 m deep [*Morin et al.*, 2010], we calculate R_T = 15.4 m^2 K W^{-1}. This comparison illustrates the interplay between climatic conditions and snowpack thermal properties, and indicates, as already suggested by [*Domine et al.*, 2007b], that within a climate change context, snow-climate feedbacks will come into play, with possible important effects on many issues, for example permafrost preservation or thawing. Indeed, the low R_T values on the tundra allowed the snow-ground interface to cool to about −19°C in late March, while with essentially similar air temperatures, the temperature of this interface in the taiga near Fairbanks barely dropped to −5°C in the winter of 2004 [*Taillandier et al.*, 2006].

[38] Unfortunately, we did not perform continuous measurements of the snow-ground interface at Barrow. However, we did so at a height of 8 cm, and this can be compared to the snow temperature measured in Fairbanks at a height of 7.5 cm in 2004 [*Taillandier et al.*, 2006]. Figure 13 shows that, even though air temperatures at Barrow and Fairbanks were similar (Figure 8b) the snow temperature at Fairbanks was 14°C higher than at Barrow, mostly because of the greater thermal insulation provided by the taiga snowpack. More efficient snowpack ventilation at Barrow may also contribute to this difference, but the effect of this process has been found to be small [*Bartlett and Lehning*, 2011; *Clifton et al.*, 2008].

5. Conclusion

[39] This study evidenced many noteworthy physical properties of the Barrow snowpack. The structure of the snowpack is largely determined by wind. In particular, the frequent wind episodes at Barrow imply that almost all layers were at some point remobilized into fairly dense wind drifts, many of which sintered to hard wind slabs. In early season, some of these wind slabs transformed into depth hoar, and this mode of formation results in depth hoar properties markedly different from those of the taiga depth hoar, which forms through different processes. We discussed that the climatic and geographic characteristics of Barrow produce snow layers of higher SSA than at other places where SSA has been studied. These data therefore indicate that predicting snow properties such as SSA based on snow type is not sufficient, and the climatic conditions must also be taken into account. Because of the high SSA of all the snow layers, the snow area index on tundra (SAI) near Barrow is higher than in other places further north or in the subarctic. The Barrow snowpack therefore efficiently traps semi-volatile compounds such as PCBs and presumably other POPs, acting as a temporary reservoir. Because of frequent diamond dust precipitation, its surface layer often has a high to very high SSA, usually between 60 and 90 m^2 kg^{-1}, which doubtlessly enhances the efficiency of this layer as a photochemical reactor, as it can efficiently adsorb gaseous species. Furthermore, this layer will contribute to an increase in snow albedo, enhancing radiative fluxes in the atmosphere above, another factor that will enhance photochemistry.

[40] The thermal resistance of the snowpack is a variable that is seldom measured. Here, we find on tundra a value of 3.25 m^2 K W^{-1}, significantly lower than in other snowpacks where this has been measured. This explains why the snow-ground interface cooled to below −19°C at Barrow. The whole snowpack was therefore at low temperatures, again an important factor to predict its chemical activity.

[41] Finally, this study stresses the intricate interplay between snow properties and climate, illustrated here with the variables SAI and thermal resistance so that snow-climate feedbacks must be accounted for in predictions of changes in Arctic climate and atmospheric chemistry.

[42] **Acknowledgments.** This work is part of the international multidisciplinary OASIS (Ocean–atmosphere-Sea Ice-Snowpack) program. It was supported by the French Polar Institute (IPEV) through grant 1017. We also benefited from the general framework of the campaign provided by the U.S. National Science Foundation, and in particular we acknowledge efficient help and support by Harry Beine through grant NSF ATM-0807702. The graphs of the auxiliary material were kindly drawn by Myriam Lacroix.

References

Bartlett, S. J., and M. Lehning (2011), A theoretical assessment of heat transfer by ventilation in homogeneous snowpacks, *Water Resour. Res.*, *47*, W04503, doi:10.1029/2010WR010008.

Cabanes, A., L. Legagneux, and F. Domine (2003), Rate of evolution of the specific surface area of surface snow layers, *Environ. Sci. Technol.*, *37*(4), 661–666, doi:10.1021/es025880r.

Calonne, N., F. Flin, S. Morin, B. Lesaffre, S. Rolland de Roscoat, and C. Geindreau (2011), Numerical and experimental investigations of the effective thermal conductivity of snow, *Geophys. Res. Lett.*, *38*, L23501, doi:10.1029/2011GL049234.

Clifton, A., C. Manes, J. D. Ruedi, M. Guala, and M. Lehning (2008), On shear-driven ventilation of snow, *Boundary Layer Meteorol.*, *126*(2), 249–261, doi:10.1007/s10546-007-9235-0.

Conger, S. M., and D. M. McClung (2009), Comparison of density cutters for snow profile observations, *J. Glaciol.*, *55*(189), 163–169, doi:10.3189/002214309788609038.

Derksen, C., A. Silis, M. Sturm, J. Holmgren, G. E. Liston, H. Huntington, and D. Solie (2009), Northwest Territories and Nunavut snow characteristics from a subarctic traverse: Implications for passive microwave remote sensing, *J. Hydrometeorol.*, *10*(2), 448–463, doi:10.1175/2008JHM1074.1.

Domine, F., and P. B. Shepson (2002), Air-snow interactions and atmospheric chemistry, *Science*, *297*(5586), 1506–1510, doi:10.1126/science.1074610.

Dominé, F., A. Cabanes, and L. Legagneux (2002), Structure, microphysics, and surface area of the Arctic snowpack near Alert during the ALERT 2000 campaign, *Atmos. Environ.*, *36*(15–16), 2753–2765, doi:10.1016/S1352-2310(02)00108-5.

Domine, F., R. Salvatori, L. Legagneux, R. Salzano, M. Fily, and R. Casacchia (2006), Correlation between the specific surface area and the short wave infrared (SWIR) reflectance of snow, *Cold Reg. Sci. Technol.*, *46*(1), 60–68, doi:10.1016/j.coldregions.2006.06.002.

Domine, F., A. S. Taillandier, and W. R. Simpson (2007a), A parameterization of the specific surface area of seasonal snow for field use and for models of snowpack evolution, *J. Geophys. Res.*, *112*, F02031, doi:10.1029/2006JF000512.

Domine, F., A. S. Taillandier, S. Houdier, F. Parrenin, W. R. Simpson, and T. A. Douglas (2007b), Interactions between snow metamorphism and climate: Physical and chemical aspects, in *Physics and Chemistry of Ice*, edited by W. F. Kuhs, pp. 27–46, R. Soc. of Chem., Cambridge, U. K.

Domine, F., M. Albert, T. Huthwelker, H. W. Jacobi, A. A. Kokhanovsky, M. Lehning, G. Picard, and W. R. Simpson (2008), Snow physics as relevant to snow photochemistry, *Atmos. Chem. Phys.*, *8*(2), 171–208, doi:10.5194/acp-8-171-2008.

Domine, F., A.-S. Taillandier, A. Cabanes, T. A. Douglas, and M. Sturm (2009), Three examples where the specific surface area of snow increased over time, *Cryosphere*, *3*(1), 31–39, doi:10.5194/tc-3-31-2009.

Domine, F., J. Bock, S. Morin, and G. Giraud (2011a), Linking the effective thermal conductivity of snow to its shear strength and its density, *J. Geophys. Res.*, *116*, F04027, doi:10.1029/2011JF002000.

Domine, F., J. C. Gallet, M. Barret, S. Houdier, D. Voisin, T. Douglas, J. D. Blum, H. Beine, and C. Anastasio (2011b), The specific surface area and chemical composition of diamond dust near Barrow, Alaska, *J. Geophys. Res.*, *116*, D00R06, doi:10.1029/2011JD016162.

Fierz, C., R. L. Armstrong, Y. Durand, P. Etchevers, E. Greene, D. M. McClung, K. Nishimura, P. K. Satyawali, and S. A. Sokratov (2009), The International classification for seasonal snow on the ground, *Rep. IACS Contrib. 1*, 80 pp., UNESCO-IHP, Paris.

Flanner, M. G., and C. S. Zender (2006), Linking snowpack microphysics and albedo evolution, *J. Geophys. Res.*, *111*, D12208, doi:10.1029/2005JD006834.

Gallet, J.-C., F. Domine, C. S. Zender, and G. Picard (2009), Measurement of the specific surface area of snow using infrared reflectance in an integrating sphere at 1310 and 1550 nm, *Cryosphere*, *3*(2), 167–182, doi:10.5194/tc-3-167-2009.

Girard, E., and J. P. Blanchet (2001), Microphysical parameterization of arctic diamond dust, ice fog, and thin stratus for climate models, *J. Atmos. Sci.*, *58*(10), 1181–1198, doi:10.1175/1520-0469(2001)058<1181:MPOADD>2.0.CO;2.

Hall, A. (2004), The role of surface albedo feedback in climate, *J. Clim.*, *17*(7), 1550–1568, doi:10.1175/1520-0442(2004)017<1550:TROSAF>2.0.CO;2.

Legagneux, L., A. Cabanes, and F. Domine (2002), Measurement of the specific surface area of 176 snow samples using methane adsorption at 77 K, *J. Geophys. Res.*, *107*(D17), 4335, doi:10.1029/2001JD001016.

Ling, F., and T. J. Zhang (2006), Sensitivity of ground thermal regime and surface energy fluxes to tundra snow density in northern Alaska, *Cold Reg. Sci. Technol.*, *44*(2), 121–130, doi:10.1016/j.coldregions.2005.09.002.

Ling, F., and T. J. Zhang (2007), Modeled impacts of changes in tundra snow thickness on ground thermal regime and heat flow to the atmosphere in Northernmost Alaska, *Global Planet. Change*, *57*(3–4), 235–246, doi:10.1016/j.gloplacha.2006.11.009.

Morin, S., F. Domine, L. Arnaud, and G. Picard (2010), In-situ measurement of the effective thermal conductivity of snow, *Cold Reg. Sci. Technol.*, *64*, 73–80, doi:10.1016/j.coldregions.2010.02.008.

Riche, F., and M. Schneebeli (2010), Microstructural change around a needle probe to measure thermal conductivity of snow, *J. Glaciol.*, *56*(199), 871–876, doi:10.3189/002214310794457164.

Sihvola, A., and M. Tiuri (1986), Snow fork for field determination of the density and wetness profiles of a snow pack, *IEEE Trans. Geosci. Remote Sens.*, *24*(5), 717–721, doi:10.1109/TGRS.1986.289619.

Sturm, M., and C. S. Benson (1997), Vapor transport, grain growth and depth-hoar development in the subarctic snow, *J. Glaciol.*, *43*(143), 42–59.

Sturm, M., and J. B. Johnson (1992), Thermal-conductivity measurements of depth hoar, *J. Geophys. Res.*, *97*(B2), 2129–2139, doi:10.1029/91JB02685.

Sturm, M., and G. E. Liston (2003), The snow cover on lakes of the Arctic Coastal Plain of Alaska, USA, *J. Glaciol.*, *49*(166), 370–380, doi:10.3189/172756503781830539.

Sturm, M., J. Holmgren, and G. E. Liston (1995), A seasonal snow cover classification-system for local to global applications, *J. Clim.*, *8*(5), 1261–1283, doi:10.1175/1520-0442(1995)008<1261:ASSCCS>2.0.CO;2.

Sturm, M., J. Holmgren, M. Konig, and K. Morris (1997), The thermal conductivity of seasonal snow, *J. Glaciol.*, *43*(143), 26–41.

Sturm, M., D. K. Perovich, and J. Holmgren (2002), Thermal conductivity and heat transfer through the snow on the ice of the Beaufort Sea, *J. Geophys. Res.*, *107*(C10), 8043, doi:10.1029/2000JC000409.

Taillandier, A. S., F. Domine, W. R. Simpson, M. Sturm, T. A. Douglas, and K. Severin (2006), Evolution of the snow area index of the subarctic snowpack in central Alaska over a whole season. Consequences for the air to snow transfer of pollutants, *Environ. Sci. Technol.*, *40*(24), 7521–7527, doi:10.1021/es060842j.

Taillandier, A. S., F. Domine, W. R. Simpson, M. Sturm, and T. A. Douglas (2007), Rate of decrease of the specific surface area of dry snow: Isothermal and temperature gradient conditions, *J. Geophys. Res.*, *112*, F03003, doi:10.1029/2006JF000514.

Tape, K. D., N. Rutter, H. P. Marshall, R. Essery, and M. Sturm (2010), Recording microscale variations in snowpack layering using near-infrared photography, *J. Glaciol.*, *56*(195), 75–80, doi:10.3189/002214310791190938.

Tape, W. (Ed.) (1994), *Atmospheric Halos*, *Atmos. Res. Ser.*, vol. 64, 143 pp., AGU, Washington, D. C.

Warren, S. G., and W. J. Wiscombe (1980), A model for the spectral albedo of snow. 2. Snow containing atmospheric aerosols, *J. Atmos. Sci.*, *37*(12), 2734–2745, doi:10.1175/1520-0469(1980)037<2734:AMFTSA>2.0.CO;2.

Warren, S. G., R. E. Brandt, and P. O. Hinton (1998), Effect of surface roughness on bidirectional reflectance of Antarctic snow, *J. Geophys. Res.*, *103*(E11), 25,789–25,807, doi:10.1029/98JE01898.

Zhang, T. J. (2005), Influence of the seasonal snow cover on the ground thermal regime: An overview, *Rev. Geophys.*, *43*, RG4002, doi:10.1029/2004RG000157.

J. Bock and F. Domine, Takuvik Joint International Laboratory, Université Laval and CNRS, 1045 avenue de La Médecine Québec, QC G1V 0A6, Canada. (florent.domine@gmail.com)

J.-C. Gallet, Norwegian Polar Institute, Fram Centre, N-9296 Tromsø, Norway.

S. Morin, Météo-France/CNRS, CNRM-GAME, CEN, 1441, rue de la Piscine, F-38400 St Martin d'Hères, France.